Icarus 441 (2025) 116674

Contents lists available at ScienceDirect

Icarus

journal homepage: www.elsevier.com/locate/icarus

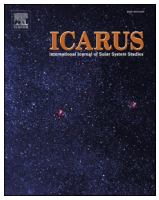

Degradation of beta-carotene under mineral thin sections during proton irradiation monitored in situ by Raman spectroscopy

Frédéric Foucher [a,b,*], Mickael Baqué [c], Aurélien Canizarès [a], Rebecca Martellotti [b,d], Jean-Pierre P. de Vera [e], Thierry Sauvage [a], Paul Sigot [a], Olivier Wendling [a], Aurélien Bellamy [a], William Hate [a], Frances Westall [b]

[a] CNRS, Université d'Orléans, CEMHTI, UPR 3079, Orléans, France
[b] CNRS, Université d'Orléans, CBM, UPR 4301, Orléans, France
[c] German Aerospace Center (DLR), Institute for Planetary Research, Berlin, Germany
[d] University of Trieste, Italy
[e] German Aerospace Center (DLR), Space Operations and Astronaut Training, MUSC, Köln, Germany

ARTICLE INFO

Keywords:
Raman spectroscopy
Beta-carotene
Particle irradiation
Radiation on Mars

ABSTRACT

More than 3.5 billion years ago, the surface of Mars experienced habitable conditions compatible with the emergence and development of primitive microbial life. Consequently, in the absence of plate tectonics, ancient biosignatures dating back several billion years could still be present at the surface of the red planet. Nevertheless, Mars has been continuously exposed to UV radiation and solar and galactic cosmic rays, which may have degraded these putative biosignatures at the surface over time. The European Space Agency's ExoMars Rosalind Franklin mission, expected to land on Mars in 2030, is thus equipped with a drill to collect samples up to 2 m deep to increase the chances of detecting well preserved molecules.

Here, based on previous models, we first estimate the dose delivered in the first meters of Mars regolith over geological time. We then describe experiments in which beta-carotene (a pigment commonly used by microorganisms) was irradiated using a 2.8 MeV proton beam and its degradation with increasing dose studied by Raman spectroscopy, using a unique device allowing in situ measurements to be carried out within the irradiation chamber. Specific sample preparation, consisting of placing a thin mineral layer on top of the pigment, was also developed to take into account the dose distribution profile within the sample. Finally, based on the dose estimated for Mars, we correlate the change in the Raman signal-to-noise ratio of beta-carotene to an equivalent depth and time on Mars.

1. Introduction

Mars is considered as one of the most promising targets in the quest for extraterrestrial life in the Solar system (Cottin et al., 2017; McKay, 1997; Westall et al., 2015). Since the Mariner 4 probe in the 1960's, many missions have been sent to study the present and ancient environmental conditions at the surface of the Red Planet (Farley et al., 2020; Grotzinger et al., 2012; Klein et al., 1976), documenting liquid water forming rivers, seas and lakes during the Noachian-Early Hesperian period (c.a. 3.5 billion years ago) (Ehlmann et al., 2009; Fassett and Head-III, 2008; Grotzinger et al., 2014; Le Deit et al., 2012; Mangold et al., 2021; Poulet et al., 2005). Locally, the surface of Mars hosted habitable conditions that lasted potentially long enough to allow the emergence and development of primitive microbial life (McKay, 1997; Schulze-Makuch et al., 2008; Westall et al., 2021; Westall et al., 2015). While life could still be active in deep aquifers several hundred meters below the surface (Marais, 2010), its existence at the surface is highly speculative. On the other hand, in the absence of plate tectonics, ancient organo-mineral traces of life dating back from the Noachian could still be present at the surface.

Nevertheless, due to its low-pressure atmosphere and the absence of a magnetic field since about 3.95 Ga (Steele et al., 2023), Mars has been continuously exposed to high-energy UV radiation, solar energetic particles (SEP) and galactic cosmic rays (GCR) which may have degraded these putative biosignatures over time. UV-C radiation (down to 190 nm) degrades organics in the first millimetres by direct exposure and by

* Corresponding author at: CNRS, Université d'Orléans, CEMHTI UPR, 3079 Orléans, France.
E-mail address: frederic.foucher@cnrs.fr (F. Foucher).

https://doi.org/10.1016/j.icarus.2025.116674
Received 30 December 2024; Received in revised form 28 April 2025; Accepted 28 May 2025
Available online 31 May 2025

forming oxygen peroxide, also responsible of the oxidation of the surface giving the planet its red colour (Baqué et al., 2022; Baqué et al., 2016; Fornaro et al., 2020; Fornaro et al., 2018; Patel et al., 2004; Poch et al., 2014; Ranjan et al., 2017; Zent and McKay, 1994). SEP and GCR, although less intense, may penetrate up to several meters depth and thus alter organics and minerals with time (Baqué et al., 2017; Brandt et al., 2017; Dartnell et al., 2012; Kminek and Bada, 2006; Pavlov et al., 2012).

In order to increase the chances of detecting well-preserved organic molecules, the European Space Agency (ESA) developed the ExoMars Rosalind Franklin rover equipped with a drill to collect samples down to 2 m depth (Battistelli et al., 2004; Hickman-Lewis et al., 2020; Kereszturi et al., 2016; Vago et al., 2017). After several postponements, the launch of the mission is now scheduled for 2028, with a landing on Mars in autumn 2030. The landing site, Oxia Planum, is an ancient terrane that has been subjected to aqueous processes (either pedologic, fluvial, deltaic, littoral or marine) resulting in alteration of the originally volcanic sediments to clays. The area could have hosted ancient hydrothermal springs. Evaporitic deposits could also be present (Fawdon et al., 2024; Quantin-Nataf et al., 2021). Some of these environments are considered favourable for the emergence and development of life, and all could have hosted life. It is therefore possible that Oxia Planum could preserve traces of some form of microbial life (Vago et al., 2017; Westall et al., 2021; Westall et al., 2018; Westall et al., 2015). The rover is equipped with a suite of complementary instruments, including high-resolution cameras, optical spectrometers and a mass spectrometer (Bost et al., 2015; Vago et al., 2017). Among them, the Raman Laser Spectrometer (RLS), located within the rover, will analyse the drill cores after crushing to detect and identify organic and mineral phases (Rull et al., 2017; Rull Pérez and Martinez-Frias, 2006). Raman spectroscopy is a key instrument in astrobiology and micropaleontology since it is highly sensitive to pigments (such as carotenoids) and carbonaceous matter, although only pigments can be considered to be a true biosignatures (Baqué et al., 2016; Dartnell et al., 2012; Edwards et al., 2013; Jehlicka et al., 2009; Vitek et al., 2009; Winters et al., 2013) since carbonaceous matter is a common constituent of both biogenic and abiotic origin. Its ability to identify minerals is also important since the association of specific minerals and carbonaceous matter may constitute good evidence of biogenicity (Clodoré et al., 2024; Edwards et al., 2007; Foucher, 2019; Foucher et al., 2015; Marshall et al., 2010).

The Raman signal depends on various parameters, including the structure and format of the sample. In particular, powders produce a higher background level than uncrushed samples, mainly due to an increase in laser induced heating (Foucher et al., 2013). Defects in materials, such as those induced by particle irradiation, are also known to alter the Raman signal by increasing the background level, widening the bands and decreasing their intensity (Ammar et al., 2015; Cusick et al., 2017; Jiang et al., 2023; Synytsya et al., 2007; Yamauchi et al., 2001). Therefore, it is important to evaluate the degradation of relevant (bio-) molecules and minerals, and to study the evolution of their Raman signal as a function of sediment depth and time on Mars, in order to determine to what depth it is necessary to drill in the hopes of detecting them.

Here, we used a unique system called *RAMSESS 2* (for *RAMan SpEctroscopy for* in Situ *Studies version 2*) allowing us to study in situ the changes in the Raman signal within the irradiation chamber connected to one beamline of an electrostatic Pelletron accelerator. This device is an upgraded version of the *RAMSESS* system that was previously used to study the alteration of polymers (Canizarès et al., 2022). Based on existing models, we evaluate the dose received on Mars with depth and time and modelled those received within the samples during our irradiation experiments, carried out using a 2.8 MeV proton beam. We then developed a specific sample preparation protocol to take into account the heterogeneity of the dose within the sample, while still allowing in situ measurements to be carried out. We thus evaluated the decrease in the Raman signal-to-noise ratio of beta-carotene, deposited under different mineral thin sections, with increasing irradiation dose. Finally, based on the estimated dose in the Martian regolith as a function of depth and time, we show that the Raman signal of beta-carotene can still be detected even after exposure to a dose corresponding to billions years of irradiation of Mars down to a few tens of centimetres below the surface. This is very encouraging in the context of current and future missions dedicated to the search of traces of life on Mars.

2. Modelling

2.1. Irradiation at the surface of Mars

Mars is exposed to two main sources of particle irradiation:

- Galactic Cosmic Rays (GCR) composed of H^+ ions (protons) at 91 %, He^{2+} ions (alpha particles) at 8 % and heavy ions (mainly carbon and oxygen) at 1 % (Le Postollec et al., 2009).

- Solar Energetic Particles (SEP), emitted mainly during sporadic events (solar flares), composed of H^+ ions at 95.4 % and He^{2+} ions at 4.6 % (Takigawa et al., 2019).

These primary high-energy particles irradiate the surface of Mars after partial loss of their velocity in the atmosphere, while producing secondary particles (electrons, neutrons, photons, etc.) which can also be a source of irradiation. In order to estimate the energy spectrum of these different ionizing particles, various numerical models have been proposed (Keating et al., 2005; McKenna-Lawlor et al., 2012a, 2012b; Le Postollec et al., 2009). Protons are the transmitted particles that can reach the highest energy, up to several GeV, and are thus those most likely to penetrate deeper into the Martian regolith. Moreover, while GCR flux is a thousand times lower than SEP flux, GCR particles can be hundred times more energetic (Keating et al., 2005) and can thus penetrate deeper below the surface of Mars. The penetration depth of protons on Mars (i.e., their stopping distance or projected range) can be calculated using the SRIM software (Ziegler et al., 2010), knowing the composition of the regolith and its density. Oxia Planum, the landing site of the ExoMars mission, is rich in clays with a composition close to that of vermiculite with the formula $(Mg,Ca)_{0.7}(Mg,Fe,Al)_6(Al,Si)_8O_{22}(OH)_4{\cdot}8H_2O$ (Quantin-Nataf et al., 2021). Using this composition for the calculation, and a density of 1.52 g.cm^{-3}, corresponding to that measured by Pathfinder (Hviid et al., 1997), it is possible to estimate the penetration depth d_{Max} of protons in the Mars regolith as a function of the incident energy (Fig.1).

The effect of irradiation on materials is commonly studied as a function of the received dose, expressed in Gray (1 Gy = 1 J.kg^{-1}). It corresponds to the energy lost by the particles per unit mass of the sample and is given by:

$$D = 1.602 \times 10^{-9} \times \frac{f \times t}{\rho} \times \frac{E}{d_{Max}} \quad (1)$$

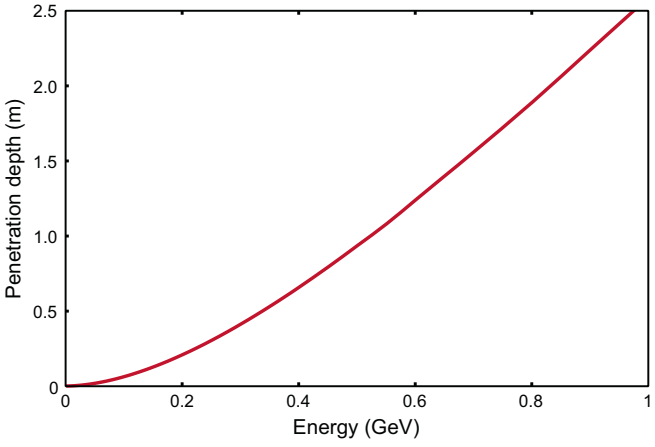

Fig. 1. Penetration depth of protons in vermiculite (density 1.52) as a function of the incident energy.

With f the flux in prot.cm^{-2}.s^{-1}, t the time in seconds, ρ the density of the sample in g.cm^{-3}, E the energy of the protons in GeV, and d_{Max} the stopping distance within the sample in meters.

Using the model from Keating et al. (2005) and the values of d_{max} displayed in Fig. 1, it is possible to estimate the dose per month associated with each energy range, and to sum them in order to calculate the total dose received by the regolith. We thus obtained a total GCR dose of 7.63 mGray/month, which is in accordance with the 7.22 mGray/month found by Le Postollec et al., 2009 and with the 6.3 ± 1.2 mGray/month given in Baqué et al. (2017).

Protons lose their energy as they travel through matter by electronic and nuclear collisions; their maximum energy is at the surface (for $d = 0$) and zero at the stopping distance (for $d = d_{Max}$). Interestingly, the energy of a proton at a depth d corresponds to its initial energy minus the energy of a proton for which the stopping distance would be d. This permits calculation of the energy loss of a proton as a function of the penetrated distance. Representative curves for different incident proton energies are shown in Fig. 2.

As shown in Fig. 2, proton energy loss (or stopping power) is not constant: its maximum is close to the implantation depth. The dose delivery is thus also heterogeneous. For a sample layer included between the depths d_i and d_{i-1}, the dose can be calculated by:

$$Dose_i = 1.602 \times 10^{-9} \times \frac{f \times t}{\rho} \times \frac{(E_i - E_{i-1})}{(d_i - d_{i-1})} \quad (2)$$

With E_i the proton energy at the depth d_i.

Finally, using the energy and fluence distributions given by Keating et al. (2005) and by Le Postollec et al., 2009 for GCR and for SEP respectively, and considering that SEP protons are only delivered at this maximum dose 3 days per terrestrial year on average, it is possible to estimate the total dose as a function of depth after a period of 3.5 Ga (Table 1). As shown in Table 1, the dose is mostly delivered by SEP in the first meter and only by GCR at greater depths.

It is important to note that these values should be considered with caution, as they are based on many approximations. In particular:

- The flux of SEP was not constant over time and was higher 2.5 billion years ago. It also depends on latitude. Thus, for a specific location, the flux varied due to the variation in the planet's obliquity over time. Finally, the flux of SEP reaching the surface also depends on atmospheric density and composition, which also changed over time.
- We used a vermiculite composition and a density 1.52 g.cm^{-3} as a model for the Martian regolith. Nevertheless, the Martian regolith and/or rocks can vary in composition and density. These variations strongly modify the particle penetration depth and therefore the dose profile (Eqs. 1 and 2).

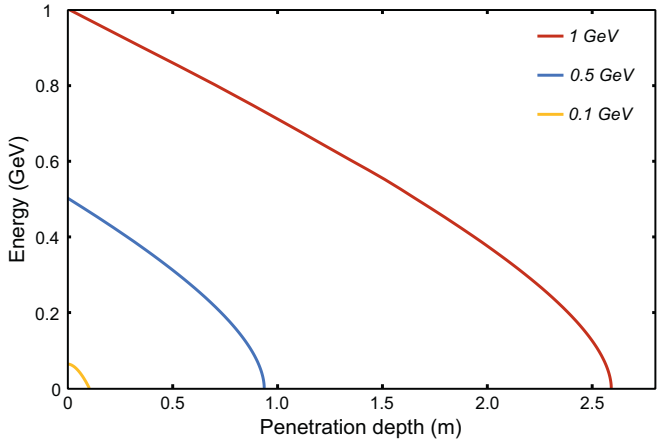

Fig. 2. Proton energy change in vermiculite (density 1.52) with penetration depth for various incident energies.

Table 1
GCR, SEP and total dose with depth in vermiculite (density 1.52) after one terrestrial year and after 3.5 Ga (terrestrial years).

Depth (m)	GCR Dose (Gy/ terrestrial year)	SEP Dose (Gy/ terrestrial year)	Total Dose (Gy/ terrestrial year)	3.5 Ga Dose (Gy)
1 cm	1.7E-04	2.3E-01	2.3E-01	**7.9E+08**
10 cm	7.9E-05	5.2E-02	5.2E-02	**1.8E+08**
50 cm	3.5E-05	4.9E-03	5.0E-03	**1.7E+07**
1 m	2.9E-05	1.5E-03	1.5E-03	**5.3E+06**
1,5 m	2.7E-05	0.0E+00	2.7E-05	**9.4E+04**
2 m	2.2E-05	0.0E+00	2.2E-05	**7.8E+04**
3 m	1.6E-05	0.0E+00	1.6E-05	**5.5E+04**
5 m	9.5E-06	0.0E+00	9.5E-06	**3.3E+04**

- The dose delivered at a given depth applies to a sample that would have remained at the same depth over time, which is obviously impossible for the periods of several billion years considered in this study. Indeed, a given sample located in the first 2 m of the Martian subsoil would have been successively exposed to the surface and/or buried several meters deep over time.
- Finally, the model does not take into account the wide variety of particles reaching the surface of Mars, nor the secondary particles created in the regolith, while the defects created by irradiation depend not only on the dose, but also on the nature (electrons, neutrons, ions, photons) and mass of the particles.

Therefore, only the order of magnitude of the dose, age and depth should be considered.

2.2. Irradiation at Pelletron

The samples used for this study were irradiated at the Pelletron facility, CEMHTI, CNRS, Orléans, using a 2.8 MeV proton beam, with a flux of 3.1 × 10^{10} prot.cm^{-2}.s^{-1} (see §3.3 for details). Since the proton beam is mono-energetic, the energy loss, and thus the dose delivery, is not homogeneous in the material volume and presents a maximum at the Bragg's peak (see Fig.4). Therefore, both duration and depth must be considered during the experiments. Table 2 shows the duration of the laboratory experiments necessary to reach a dose equivalent to 3.5 Ga of irradiation on Mars (3.5 Ga$_{ME}$, Mars Equivalent) at different Martian depths, close to the sample surface and at the Bragg's peak position. Table 2 shows the significant differences between the irradiation on Mars and experiments conducted with the Pelletron. At the Pelletron, only a few tens of microns of depth are irradiated, whereas on Mars, the particles can reach several tens of metres. In contrast, it is possible at the Pelletron to reach doses equivalent to billion years of Martian

Table 2
Total dose with depth in vermiculite (density 1.52) after 3.5 Ga$_{ME}$ on Mars at different depths, and corresponding experimental duration to reach a similar dose in laboratory using a 2.8 MeV proton beam with a flux of 3.1 × 10^{10} prot. cm^{-2}.s^{-1} for two different sample depths: close to the surface (20 μm) and at the Bragg's peak position (119 μm).

Depth on Mars	Dose on Mars after 3.5 Ga$_{ME}$ (Gy)	Duration of laboratory experiments for equivalent dose at 20 μm depth			Duration of laboratory experiments for equivalent dose at 119 μm depth		
		h	min	s	h	min	s
1 cm	7.9E+08	413	58	1	81	15	36
10 cm	1.8E+08	95	14	20	18	41	42
50 cm	1.7E+07	9	5	51	1	47	8
1 m	5.3E+06	2	45	46	0	32	32
1,5 m	9.4E+04	0	2	57	0	0	34
2 m	7.8E+04	0	2	27	0	0	29
3 m	5.5E+04	0	1	44	0	0	20
5 m	3.3E+04	0	1	2	0	0	12

irradiation in just a few hours.

3. Materials and methods

3.1. Single halite crystals

To highlight the dose heterogeneity in Pelletron-irradiated samples, single halite crystals were prepared. Indeed, defects created during irradiation are known to act as colour centres in halite associated with an increase in the background level of the Raman signal (Mao et al., 2022; Sonnenfeld, 1995). These samples were prepared by dissolving NaCl powder (*Sigma-Aldrich*) in pure *Milli-Q* water in a crystallizer and by letting the solution dry in a cold room at 4 °C for a month. We thus obtained many parallelepiped crystals. The largest one (8x8x2 mm^3) was glued onto the sample holder using double sided conductive copper tape for irradiation at the Pelletron.

3.2. Beta-carotene in between silicon and mineral layers

We focused our investigations on beta-carotene ($C_{40}H_{56}$), a molecule (and carotenoids in general) that is widely used by microorganisms to protect themselves from oxidative stresses caused by UV and particle irradiation, low or high temperatures, or salinity increase (Saubenova et al., 2024). It is thus considered as a good potential biosignature to search for on Mars (Baqué et al., 2022; Baqué et al., 2016; Dartnell et al., 2012; Patel et al., 2004; Vitek et al., 2009).

Previous studies of the alteration of biomolecules during irradiation were carried out using pellets of powder in which the molecules of interest were mixed with crushed minerals before being compressed (e.g., Baqué et al., 2016). However, this preparation is not suitable for in situ Raman analyses for several reasons. First, the heat of the sample induced by the laser of the Raman system is strongly increased on powdered samples because the thermal conductivity of powdered materials is very low (Foucher et al., 2013). Moreover, in addition to potentially altering the biomolecules, this thermal increase also leads to reduce the Raman signal-to-noise ratio (Foucher et al., 2013). Secondly, the *RAMSSES 2* device (see §3.5) is not confocal, therefore the depth of field can be of several hundreds of micrometres in transparent samples. Moreover, the intensity of the Raman signal decreases with the depth of analysis due to light absorption. Therefore, it would have been impossible to attribute a depth, and thus a dose, to the collected Raman signal. The use of a pure beta-carotene deposit was also not adapted because it would desorb under vacuum and may easily burn under the laser and/or proton beam (s).

In order to circumvent these problems, specific samples consisting of a beta-carotene layer sandwiched between a silicon wafer and a thin section of mineral were prepared. Quartz (SiO_2), gypsum ($CaSO_4{\cdot}2H_2O$) and calcite ($CaCO_3$) from the *International Space Analogue Rockstore* (Bost et al., 2013), Orléans, France (reference numbers 12FR03, 12UN03 and 12MA02, for quartz, calcite and gypsum respectively) were used since these minerals are known to fossilize and preserve microorganisms and biomolecules, and because they are transparent to green laser. Their density was measured using Archimedes' principle, giving 2.71, 2.63 and 2.30 $g.cm^{-3}$, for calcite, quartz and gypsum respectively. The penetration depth of 2.8 MeV protons calculated using SRIM software was 63 µm, 66 µm and 71 µm respectively and, therefore, self-supporting thin sections were prepared by the company *Thin Section Lab*, in Toul, France, to permit the transmission of protons to the beta-carotene layer. The thicknesses actually measured for the sections were 50 µm, 52 µm and 40 µm, for calcite, quartz and gypsum respectively.

The samples were prepared as follows. Beta-carotene powder (*Sigma-Aldrich*) was dissolved in water and droplets of these solutions were deposited in 5 mm diameter holes made in c.a. 50 µm thick *Millipore Whatman* filters placed onto silicon wafers. A glass slide, topped with a 750 g weight, was then loaded over them. After drying in air overnight at room temperature, the glass slide and the filters were removed. This allowed beta-carotene layers on silicon wafers made up of aggregates ranging from 1 to 40 µm in thickness to be obtained. The mineral thin sections were placed on top of the beta-carotene. These samples were finally pasted onto the sample holder using copper tape. A sample without a mineral thin section on top was also prepared to estimate the laser penetration depth into beta-carotene (see §4.2).

3.3. Low energy ion beam Pelletron accelerator

The irradiation experiments were carried out in the micro-beam line vacuum chamber of the CEMHTI Pelletron facility (http://emir.in2p3.fr/CEMHTI), using a 2.8 MeV proton (H^+) beam. The beam has a 5 × 5 mm^2 square shape and scans the sample surface with a Lissajous pattern to obtain a homogeneous irradiation on an 18.5 mm diameter area. The halite sample was irradiated with a flux of 5×10^{10} $prot.cm^2.s^{-1}$ for 4000 s to reach a total fluence of 2×10^{14} $prot.cm^{-2}$. The mineral/beta-carotene/silicon samples were irradiated at a flux of 3×10^{10} $prot.cm^{-2}.s^{-1}$ to reach sequentially different total fluences (2×10^{13}, 2×10^{14}, 4×10^{14}, 7×10^{14} and 20×10^{14} $prot.cm^{-2}$).

3.4. RAMSESS 2

In order to follow the evolution of samples during irradiation experiments, a self-made, in situ Raman device called *RAMSESS* (for *RAMan SpEctroscopy for* in Situ *Studies*) was developed in 2022 (Canizarès et al., 2022). While this device demonstrated the relevance of coupling a Raman spectrometer to an irradiation chamber, it used a low spatial resolution optical camera and the laser spot size was relatively large (more than 2 mm diameter at sample surface). In addition, the sample holder was not cooled. Therefore, an upgraded version of the system, called *RAMSESS 2*, was developed (see Fig. 3). It includes a new Raman probe equipped with microscope objectives probing through a vacuum window port in fused silica located at a few millimetres from the sample surface to optimize the lateral analysis resolution. This new Raman probe is an in-house made device derived from a *Renishaw RP10* probe, equipped with a white light source and a camera for optical imaging. Raman spectra were acquired with a green laser (Nd:YAG frequency doubled laser) of wavelength $\lambda = 532$ nm. The laser power was set to ca. 10 mW at the sample surface and focalized using a *Mitutoyo* objective of magnification 20× (numerical aperture *N.A.* = 0.28) for which the associated laser spot size diameter at the sample surface was measured at ca. 15 µm using the scanning-knife method (Foucher, 2021; Hauer et al., 2016). The spot size is thus relatively large and therefore limits the thermal increase induced by the laser (Foucher, 2021; Foucher et al., 2013). It is connected to a *Renishaw RA100* spectrometer (1800 $lines.mm^{-1}$ grating, 250 mm focal length) with a spectral resolution ranging from 3.5 cm^{-1} at 200 cm^{-1}, to 1.65 cm^{-1} at 3325 cm^{-1}. A thermoelectrically cooled charge-coupled device (CCD) at −50 °C ensures good stability of detection.

RAMSESS 2 also includes a new sample holder in copper, cooled down by water circulation to reduce thermal degradation of the sample potentially induced by the proton and/or laser beam(s). Due to ionoluminescence, the Raman signal cannot be acquired during irradiation. The sample holder is thus alternately moved from the irradiation position (i.e., sample surface perpendicular to the proton beam) to the Raman analysis position (i.e., perpendicular to the Raman laser beam) by a rotation of 90°. It can be moved using an (X,Y,Z) goniometer to the different sample positions. For each sample, the laser focus was first made on the mineral surface using the optical camera. Then, the samples were moved vertically and along X and Y in order to obtain positions for which the Raman signal of beta-carotene is maximum. After each irradiation, the sample holder was moved a few µm in X, Y and Z around these optimal positions in order to obtain again the maximum Raman signal and to correct the repositioning deviations of the stage, mainly due to the rotation between the "irradiation" position and the "Raman" position.

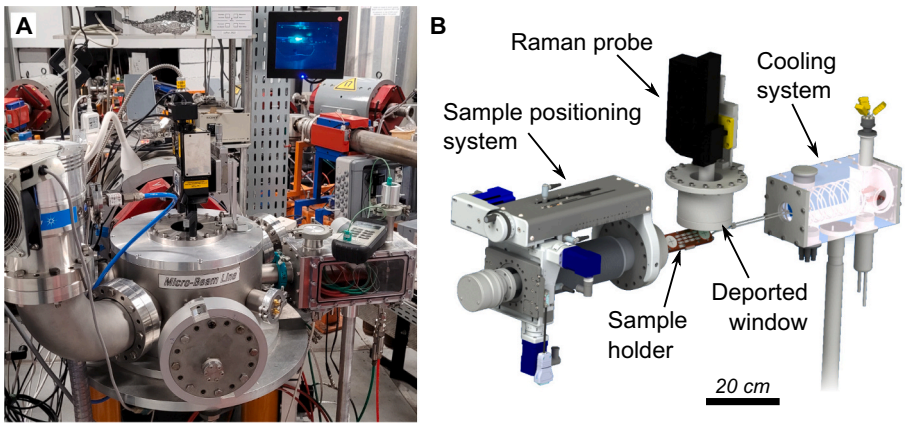

Fig. 3. *RAMSESS 2* device. (A) Photograph of the device and (B) associated schematics.

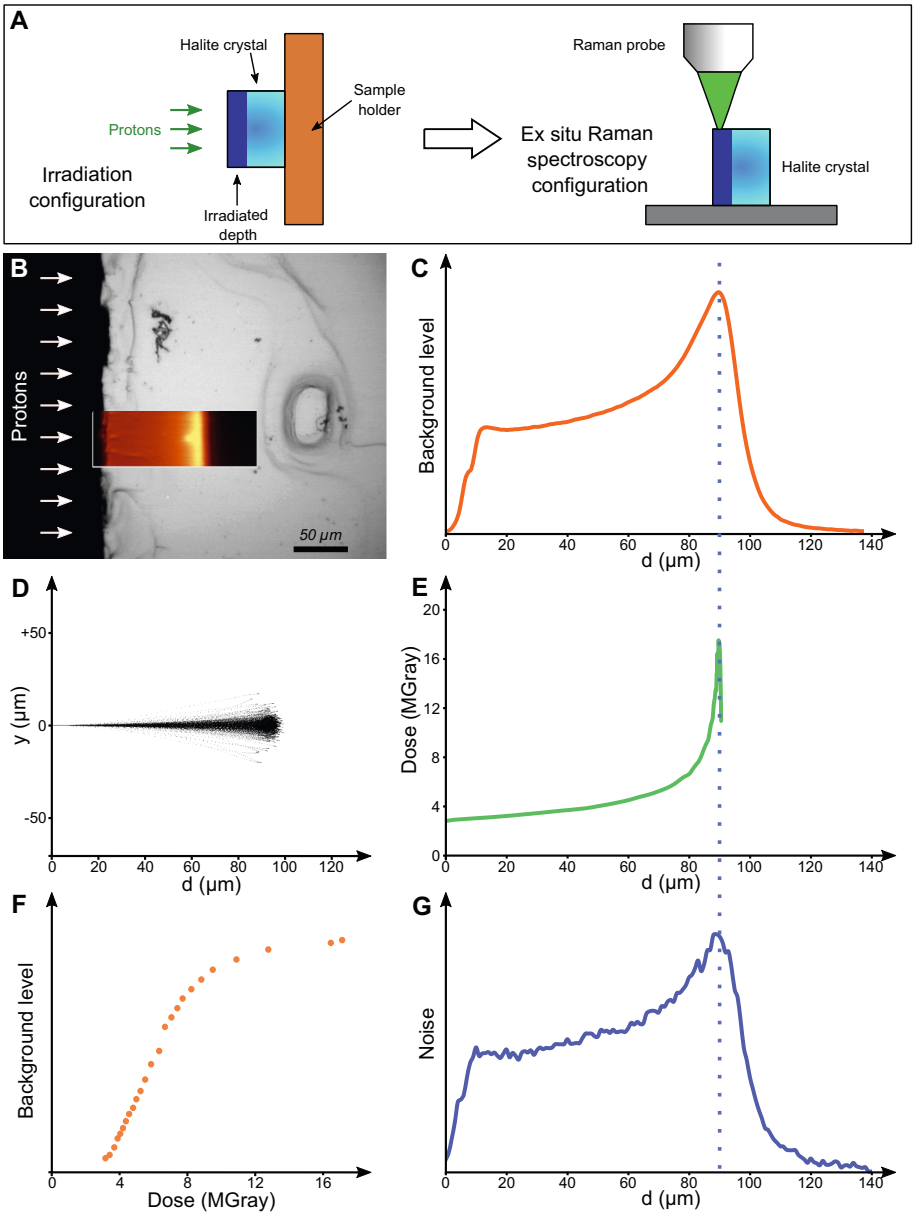

Fig. 4. Irradiated halite crystal. (A) Schematics of the halite crystal configurations during proton irradiation then during ex situ Raman analysis. (B) Raman map of the background level overlain on the optical photograph of the sample viewed from above, and (C) associated average intensity of the background level. (D) SRIM simulation and (E) equivalent dose for 4000 s. (F) Background level versus the dose. (G) Noise on the Raman signal between 600 and 3600 cm^{-1}.

After the experiment, the Raman spectra were processed as follows:

- Only the spectral range between 800 cm^{-1} and 1800 cm^{-1} was considered.
- The spectra were normalized to their minimum value (usually located at 800 cm^{-1}). Since the signal intensity at this point is mainly influenced by the focusing of the system, this allows for correction of the focusing shift between two irradiations.
- The background was subtracted using a second order polynomial.

3.5. Ex situ Raman spectroscopy

High resolution Raman spectroscopy analyses were carried out on the halite sample after irradiation and on beta-carotene deposited on silicon wafer using a *WITec Alpha 500RA* system, at the CEMHTI laboratory, CNRS, Orléans, France, equipped with a green laser (Nd:YAG frequency doubled laser) of wavelength $\lambda = 532$ nm. The laser power was set to 14 mW at sample surface. Raman maps were acquired using a *Nikon E Plan* objective of magnification 20× (numerical aperture *N.A.* = 0.40), for which the associated laser spot size diameter at the sample surface was measured to 2.4 µm (Foucher, 2021). Raman spectra were acquired using a 600 $g.mm^{-1}$ grating spectrometer ranging from approximately 70 to 3800 cm^{-1}, and a resolution ranging from 3 to 5 cm^{-1}.

4. Results

4.1. Raman map of irradiated halite crystal

A Raman map of the halite single crystal was acquired ex situ after irradiation on one of the sides perpendicular to the irradiated surface of the crystal. Fig. 4 displays the increase in the background level, corresponding to the area below the spectrum measured between 1400 and 2400 cm^{-1}, and of the noise, corresponding to the number of CCD counts between the maximal and the minimal value of the signal after removal of the baseline on the same wavenumber range, as well as the dose calculated using SRIM simulations. The correlation between the dose (i.e., the number of defects in the material) and the changes in the Raman signal (background and noise levels) is clearly shown. A saturation is observed on the background level for doses higher than about 10 MGy. The signal defect near the sample surface is explained by the irregularities and roughness of the crystal edge, the depth of field of the optical system and the dimensions of the laser spot.

4.2. Raman signal of silicon through beta-carotene powder

In order to estimate the penetration depth of the green laser into beta-carotene, and therefore the maximal depth over which the Raman signal is collected, beta-carotene powder was deposited at the surface of a silicon wafer. Then, using the *WITec Alpha 500RA* system, the Raman signal of silicon was collected through different thickness of beta-carotene (i.e., through grains of different sizes) and we observed that silicon is no longer detected through a beta-carotene thickness of more than 2 µm. This is in accordance with the absorbance value of beta-carotene found in the literature (e.g., Lee et al., 2019). Therefore, it is possible to conclude that the Raman signal of beta-carotene measured using a 532 nm green laser is associated to the first 2 µm of beta-carotene at its maximum, whatever the depth of field of the system (i.e., with *RAMSESS 2* as well), and whatever the layer thickness.

4.3. Raman signal of beta-carotene under minerals collected in situ during proton irradiation

The evolution of the Raman signal of beta-carotene acquired in situ within the irradiation chamber for increasing fluence in the different samples is displayed in Fig. 5.

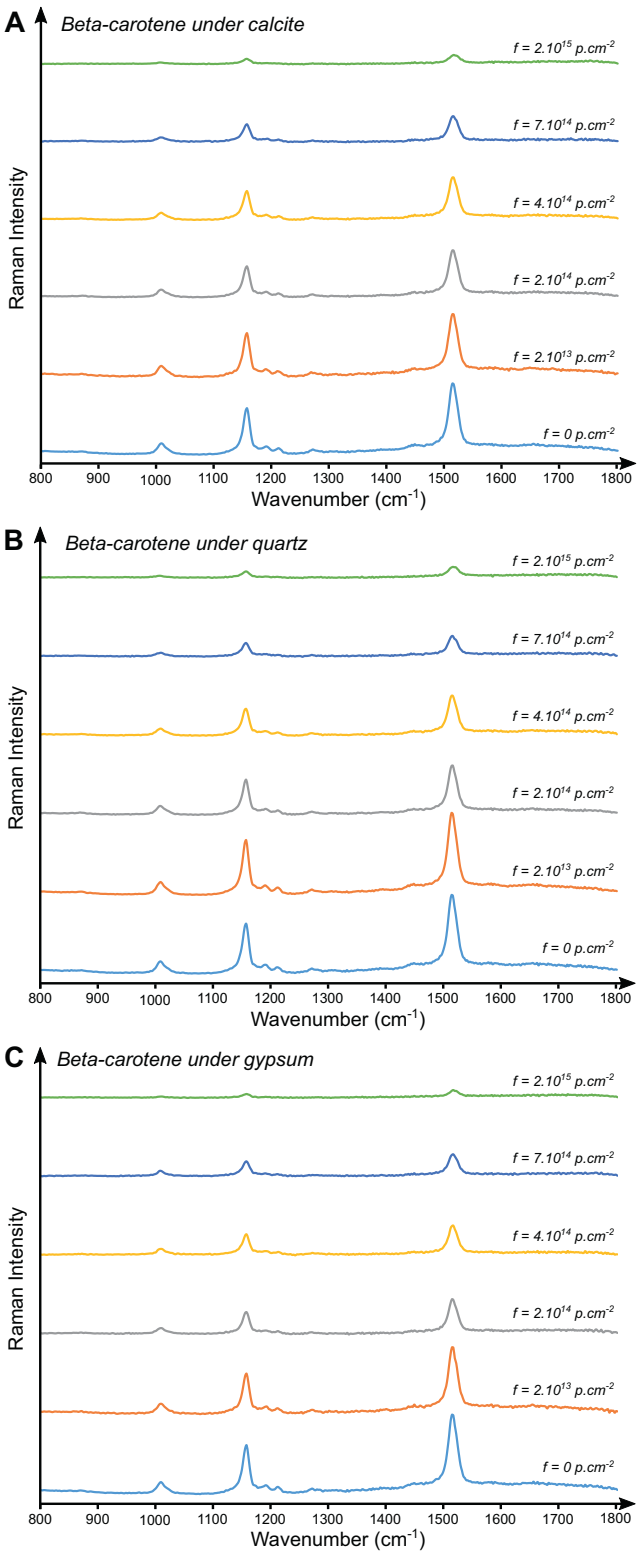

Fig. 5. Raman spectra of beta-carotene under (A) calcite (B) quartz and (C) gypsum thin sections, acquired in situ within the irradiation chamber at different fluences.

5. Discussion

The very good correlation between the profile of the dose obtained from SRIM simulations and the noise and background level Raman spectral maps, representative of the defects created under irradiation,

observed ex situ on the halite crystal (Fig. 4), demonstrates the importance of taking into account the analysis depth in nuclear particles irradiation experiments, such protons. Thus, when analysing the irradiated surface of samples by Raman spectroscopy, it is important to evaluate the penetration depth of the laser into the sample and the depth of field of the objective used, in order to correctly estimate the depth and thickness of the analysed layer and to correctly determine the associated dose.

To circumvent this effect, we preferred to develop a specific sample preparation protocol where the pure pigment is deposited on a silicon wafer before being covered by a thin mineral layer with good laser transmission efficiency. This allows us to perfectly correlate the Raman signal to a given dose while avoiding heating and desorption/sputtering of beta-carotene under vacuum. Our measurements show that the laser penetration depth in beta-carotene is 2 µm, which means that the Raman signal is collected at most in the first 2 µm of beta-carotene in the layer, regardless of its total thickness. In addition, the depth of field of the *RAMSESS 2* system is several hundred micrometres (i.e., greater than the maximum 40 µm thickness of the beta-carotene layer). Therefore, the Raman signal is collected over the entire depth of the sample (i.e., the mineral lamina, the beta-carotene layer, and the silicon wafer) and its intensity does not depend on the distance between the mineral section and the beta-carotene layer (see Fig. 6A).

Based on SRIM simulations, we estimate the dose delivered per second, for a flux of 3×10^{10} prot.cm^{-2} s^{-1}, in the different samples (see Fig. 6). For calcite and quartz, the Bragg's peak is located in the beta-carotene layer, whereas for the gypsum sample it is located in the silicon wafer. There is a dose shift at each interface since the dose depends on the elementary composition and on the density of the materials.

In Fig. 6B-6D, the beta-carotene layer is represented as an homogeneous layer of 40 µm thickness, although it comprises particles of various sizes, where those of less than 40 µm are located deeper and do not touch the mineral section (Fig. 6A). Nevertheless, the particles' energy is not modified in vacuum, meaning that the dose received in the first micrometres of beta-carotene is the same, whatever the grain size. Moreover, as stated above, only the first 2 µm of beta-carotene is analysed by Raman spectroscopy and, due to the large depth of field of the *RAMSESS 2* system, the Raman signal intensity is not modified by the distance between the mineral and the beta-carotene layer. It is thus possible to associate the Raman signal collected from beta-carotene with the dose calculated for the first 2 µm.

Finally, it is shown that for a flux of 3.10^{10} prot.cm^{-2}.s^{-1}, the dose rates in the first 2 µm of beta-carotene are of 1220, 1235 and 895 Gray.s^{-1}, under the calcite, quartz and gypsum thin sections respectively.

To correlate the decrease in the Raman signal-to-noise ratio of beta-carotene observed in Fig. 5 with the dose, the Raman intensity of the peak at 1515 cm^{-1} was divided by the noise calculated on the 1700–1800 cm^{-1} part of the Raman signal (i.e., a part without Raman bands). This noise corresponds to the standard deviation of the intensity, after removing of the base line. Finally, using Table 2, it is possible to compare the experimental dose to that on Mars, and to display the change in the signal-to-noise ratio of beta-carotene with depth after 3.5 Ga_{ME}, or with time at a given depth (10 cm for example), as displayed in Fig. 7.

The signal to noise ratio of beta-carotene decreases with increasing irradiation dose; it is reduced of up to 86 %, 89 % and 80 % for calcite, quartz and gypsum respectively. This decrease is a combination of the decrease in the Raman signal of beta-carotene (Fig. 5) and the increase of the noise (Fig. 4). It is important to note that, even before irradiation, the signal to noise ratio varies from one mineral to another since they are more or less transparent to the laser. Unlike halite, measurements on quartz, calcite, and gypsum crystals (personal data not shown here) have shown that their laser absorption properties are not significantly altered by irradiation.

The results demonstrate that the signal of beta-carotene on Mars at 10 cm depth would rapidly decrease in the first 500 million years (Mars equivalent), but would be still detectable after 1.5 Ga_{MA}. More interestingly, even after 3.5 Ga_{MA} of Martian irradiation, the signal would remain very high below 1 m and would be almost unaltered below 1.5 m (Figs. 5 and 7). These results are very encouraging in the context of current and future missions dedicated to the search of traces of life on Mars. Indeed, this means that the ExoMars drill could potentially detect

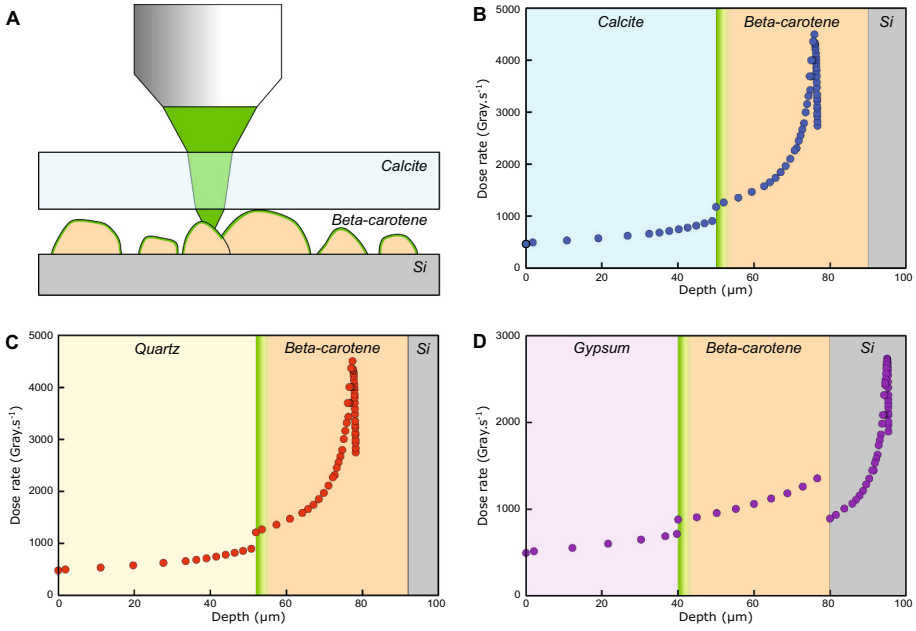

Fig. 6. (A) Schematic view of the samples during in situ Raman acquisition. Due to the absorption of beta-carotene, the signal is collected in the first 2 µm (in green) under the mineral layer (here calcite), whatever the powdered grain size. (B–D) Dose rate in Gray.s^{-1} for a flux of 3.10^{10} prot.cm^{-2}.s^{-1} within a sample made of a 40 µm thick beta-carotene layer deposited on silicon under a layer of (A) calcite, (B) quartz and (C) gypsum. In reality, since the layer of beta-carotene comprises grains of various sizes, the dose in the silicon wafer may be different. Nevertheless, the dose is almost constant in the thickness of beta-carotene analysed by Raman spectroscopy (2 µm, in green) whatever the size of the grains. (For interpretation of the references to colour in this figure legend, the reader is referred to the web version of this article.)

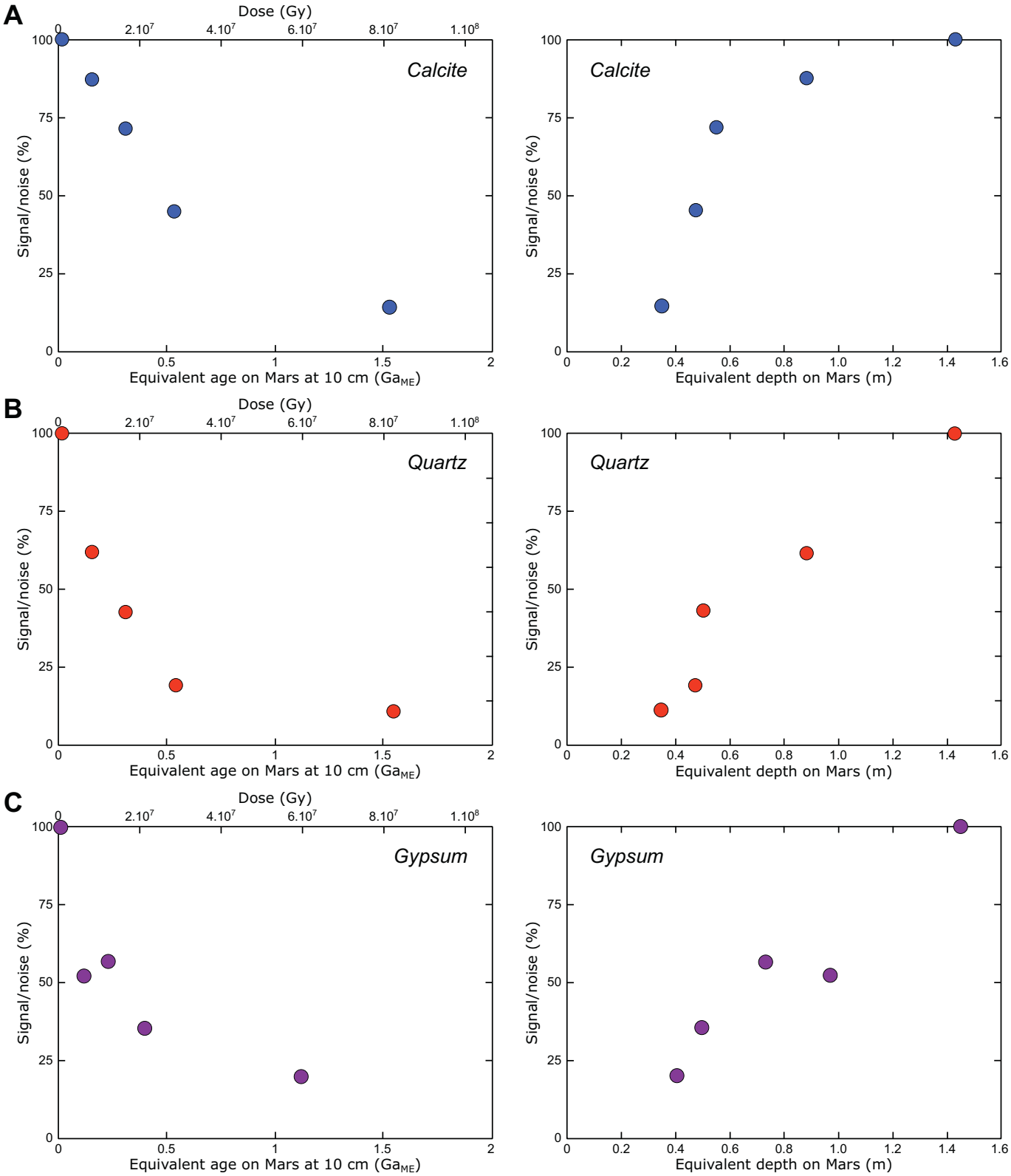

Fig. 7. Normalized Raman signal to noise ratio of the 1515 cm^{-1} Raman band of beta-carotene versus the age (and the dose) at 10 cm depth and versus the depth after 3.5 Ga of Martian irradiation under (A) calcite, (B) quartz and (C) gypsum.

well-preserved pigments at depths up to 2 m, which would constitute indisputable proof of extraterrestrial life. It is, nevertheless, important to note that the results of these experiments, and the model used, rely on numerous approximations. In particular, complementary experiments must be carried out with other types of particles (e.g., heavy ions) and different energies, in order to evaluate the effect of these parameters on the degradation of the molecules.

Finally, the proposed sample preparation protocol, consisting of trapping beta-carotene between silicon and a thin mineral layer, proves to be very relevant and efficient. A specific sample container based on

this architecture is currently under study for the irradiation of a wide variety of other molecules.

6. Conclusion

Using an in-house developed device called *RAMSESS 2*, we were able to follow the alteration of beta-carotene under proton irradiation, in situ within the irradiation chamber. A specific sample preparation protocol has been designed allowing to accurately link the Raman signal and the dose. Then, using existing models, we evaluated the equivalent dose delivered in the first meters of Martian regolith over several billion years. Finally, we correlated the change in the signal-to-noise ratio of beta-carotene with the depth and/or the equivalent age on Mars, and showed that this pigment could theoretically be detected at Oxya Planum, in the drill cores that will be collected during the future ExoMars mission.

Similar experiments will be carried out to assess the effects of radiation on other types of samples and biomolecules. In addition, they will be supplemented by other irradiation experiments, using other particles, the alteration of matter under irradiation depending both on the dose and on the mass of the incident particles.

CRediT authorship contribution statement

Frédéric Foucher: Writing – original draft, Project administration, Methodology, Investigation, Funding acquisition, Formal analysis, Data curation, Conceptualization. **Mickael Baqué:** Writing – review & editing, Investigation. **Aurélien Canizarès:** Writing – review & editing, Methodology, Investigation, Conceptualization. **Rebecca Martellotti:** Writing – review & editing, Investigation, Formal analysis. **Jean-Pierre P. de Vera:** Writing – review & editing, Investigation. **Thierry Sauvage:** Writing – review & editing, Validation, Methodology, Formal analysis, Conceptualization. **Paul Sigot:** Visualization, Resources, Conceptualization. **Olivier Wendling:** Resources, Investigation, Conceptualization. **Aurélien Bellamy:** Resources, Conceptualization. **William Hate:** Resources. **Frances Westall:** Writing – review & editing, Validation.

Declaration of competing interest

The authors declare that they have no known competing financial interests or personal relationships that could have appeared to influence the work reported in this paper.

Acknowledgments

We thank CNES for funding. We thank the EMIR&A network for support.

Data availability

Data will be made available on request.

References

Ammar, M.R., Galy, N., Rouzaud, J.-N., Toulhoat, N., Vaudey, C.E., Simon, P., Moncoffre, N., 2015. Characterizing various types of defects in nuclear graphite using Raman scattering: heat treatment, ion irradiation and polishing. Carbon 95, 364–373.

Baqué, M., Verseux, C., Böttger, U., Rabbow, E., Vera, J.P.P., Billi, D., 2016. Preservation of biomarkers from cyanobacteria mixed with Mars like regolith under simulated Martian atmosphere and UV flux. In: Origin of Life and Evolution of the Biosphere, 46, pp. 289–310.

Baqué, M., Dobrijevic, M., Postolle, A.L., Moreau, T., Faye, C., Vigier, F., Incerti, S., Coussot, G., Caron, J., Vandenabeele-Trambouze, O., 2017. Irradiation effects on antibody performance in the frame of biochip-based instruments development for space exploration. Int. J. Astrobiol. 16, 82–90.

Baqué, M., Backhaus, T., Meeßen, J., Hanke, F., Böttger, U., Ramkissoon, N., Olsson-Francis, K., Baumgärtner, M., Billi, D., Cassaro, A., de la Torre Noetzel, R., Demets, R., Edwards, H., Ehrenfreund, P., Elsaesser, A., Foing, B., Foucher, F., Huwe, B., Joshi, J., Kozyrovska, N., Lasch, P., Lee, N., Leuko, S., Onofri, S., Ott, S., Pacelli, C., Rabbow, E., Rothschild, L., Schulze-Makuch, D., Selbmann, L., Serrano, P., Szewzyk, U., Verseux, C., Wagner, D., Westall, F., Zucconi, L., de Vera, J.-P.P., 2022. Biosignature stability in space enables their use for life detection on Mars. Sci. Adv. 8, eabn7412.

Battistelli, E., Bini, A., Cisbani, A., Cosi, M., Falciani, P., Preti, G., 2004. Scientific instruments studied by Galileo Avionica for Mars surface exploration. Planet. Space Sci. 52, 47–53.

Bost, N., Westall, F., Ramboz, C., Foucher, F., Pullan, D., Meunier, A., Petit, S., Fleischer, I., Klingelhöfer, G., Vago, J., 2013. Missions to Mars: characterisation of Mars analogue rocks for the international space analogue Rockstore (ISAR). Planet. Space Sci. 82–83, 113–127.

Bost, N., Ramboz, C., Breton, N.L., Foucher, F., Lopez-Reyes, G., Angelis, S.D., Josset, M., Venegas, G., Sanz-Arranz, A., Pérez, F.R., Medina, J., Josset, J.-L., Souchon, A., Ammannito, E., Carli, C., Vago, J.L., Westall, F., 2015. Testing the ability of the ExoMars 2018 payload to document geological context and potential habitability on Mars. Planet. Space Sci. 108, 87–97.

Brandt, A., Meeßen, J., Jänicke, R.U., Raguse, M., Ott, S., 2017. Simulated space radiation: impact of four different types of high-dose ionizing radiation on the lichen Xanthoria elegans. Astrobiology 17 (2), 136–144.

Canizarès, A., Foucher, F., Baqué, M., de Vera, J.-P., Sauvage, T., Wendling, O., Bellamy, A., Sigot, P., Georgelin, T., Simon, P., Westall, F., 2022. In situ Raman spectroscopy monitoring of material changes during proton irradiation. Appl. Spectrosc. 76, 723–729.

Clodoré, L., Foucher, F., Hickman-Lewis, K., Sorieul, S., Jouve, J., Réfrégiers, M., Collet, G., Petoud, S., Gratuze, B., Westall, F., 2024. Multi-technique characterization of 3.45 Ga microfossils on earth: a key approach to detect possible traces of life in returned Samples from Mars. Astrobiology 24 (2), 190–226.

Cottin, H., Kotler, J.M., Bartik II, K., Cockell, C.S., Vera, J.P.P., Ehrenfreund, P., Leuko, S., Kate, I.L.T., Martins, Z., Pascal, R., Quinn, R., Rettberg, P., Westall, F., 2017. Astrobiology and the possibility of life on earth and elsewhere. Space Science Review 209, 1–42.

Cusick, A.B., Lang, M., Zhang, F., Sun, K., Li, W., Kluth, P., Trautmann, C., Ewing, R.C., 2017. Amorphization of Ta2O5 under swift heavy ion irradiation. Nucl. Instrum. Methods Phys. Res., Sect. B 407, 25–33.

Dartnell, L.R., Page, K., Jorge-Villar, S.E., Wright, G., Munshi, T., Scowen, I.J., Ward, J. M., Edwards, H.G.M., 2012. Destruction of Raman biosignatures by ionising radiation and the implications for life detection on Mars. Anal. Bioanal. Chem. 403, 131–144.

Edwards, H.G.M., Jorge-Villar, S.E., Pullan, D., Hargreaves, M.D., Hofmann, B., Westall, F., 2007. Morphological biosignatures from relict fossilised sedimentary geological specimens: a Raman spectroscopic study. J. Raman Spectrosc. 38, 1352–1361.

Edwards, H.G.M., Hutchinson, I., Ingley, R., Parnell, J., Vitek, P., Jehlicka, J., 2013. Raman spectroscopic analysis of geological and biogeological specimens of relevance to the ExoMars Mission. Astrobiology 13 (6), 543–549.

Ehlmann, B.L., Mustard, J.F., Swayze, G.A., Clark, R.N., Bishop, J.L., Poulet, F., Marais, D.J.D., Roach, L.H., Milliken, R.E., Wray, J.J., Barnouin-Jha, O., Murchie, S. L., 2009. Identification of hydrated silicate minerals on Mars using MRO-CRISM: geologic context near Nili Fossae and implications for aqueous alteration. J. Geophys. Res. 114, 33. E00D08.

Farley, K.A., Williford, K.H., Stack, K.M., Bhartia, R., Chen, A., de la Torre, M., Hand, K., Goreva, Y., Herd, C.D.K., Hueso, R., Liu, Y., Maki, J.N., Martinez, G., Moeller, R.C., Nelessen, A., Newman, C.E., Nunes, D., Ponce, A., Spanovich, N., Willis, P.A., Beegle, L.W., Bell, J.F., Brown, A.J., Hamran, S.-E., Hurowitz, J.A., Maurice, S., Paige, D.A., Rodriguez-Manfredi, J.A., Schulte, M., Wiens, R.C., 2020. Mars 2020 Mission overview. Space Sci. Rev. 216, 142.

Fassett, C.I., Head-III, J.W., 2008. Valley network-fed, open-basin lakes on Mars: distribution and implications for Noachian surface and subsurface hydrology. Icarus 198, 37–56.

Fawdon, P., Orgel, C., Adeli, S., Balme, M., Calef, F.J., Davis, J.M., Frigeri, A., Grindrod, P., Hauber, E., Le Deit, L., Loizeau, D., Nass, A., Quantin-Nataf, C., Sefton-Nash, E., Thomas, N., Torres, I., Vago, J.L., Volat, M., De Witte, S., Altieri, F., Apuzzo, A., Aramendia, J., Arana, G., Bahia, R.S., Banham, S.G., Barnes, R., Barrett, A.M., Benedix, W.-S., Bhardwaj, A., Boazman, S.J., Bontognali, T.R.R., Bridges, J., Bultel, B., Ciarletti, V., De Sanctis, M.C., Dickeson, Z., Favaro, E.A., Ferrari, M., Foucher, F., Goetz, W., Haldemann, A.F.C., Harrington, E., Kapatza, A., Koschny, D., Krzesinska, A.M., Le Gall, A., Lewis, S.R., Lim, T., Madariaga, J.M., Man, B.J., Mandon, L., Mangold, N., Martin-Torres, J., McNeil, J.D., Molina, A., Moral, A.G., Motaghian, S., Nikiforov, S., Oudart, N., Pacifici, A., Parkes Bowen, A., Plettemeier, D., Poulakis, P., Putri, A.R.D., Ruesch, O., Sam, L., Schröder, C., Statz, C., Thomas, R., Tirsch, D., Toth, Z., Turner, S., Voelker, M., Werner, S.C., Westall, F., Whiteside, B.J., Williams, A., Williams, R.M.E., Wright, J., Zorzano, M.-P., 2024. The high-resolution map of Oxia Planum, Mars; the landing site of the ExoMars Rosalind Franklin rover mission. J. Maps 20, 2302361.

Fornaro, T., Boosman, A., Brucato, J.R., Ten Kate, I.L., Siljeström, S., Poggiali, G., Steele, A., Hazen, R.M., 2018. UV irradiation of biomarkers adsorbed on minerals under Martian-like conditions: hints for life detection on Mars. Icarus 313, 38–60.

Fornaro, T., Brucato, J.R., Poggiali, G., Corazzi, M.A., Biczysko, M., Jaber, M., Foustoukos, D.I., Hazen, R.M., Steele, A., 2020. UV irradiation and near infrared characterization of laboratory Mars soil analog samples. Front. Astron. Space Sci. 7, 539289.

Foucher, F., 2019. Detection of biosignatures using Raman spectroscopy. In: Cavalazzi, B., Westall, F. (Eds.), Biosignatures for Astrobiology, Advances in Astrobiology and Biogeophysics. Springer International Publishing, pp. 267–282.

Foucher, F., 2021. Influence of laser shape on thermal increase during micro-Raman spectroscopy analyses. J. Raman Spectrosc. 53 (3), 664–676.
Foucher, F., Lopez-Reyes, G., Bost, N., Rull-Perez, F., Rüßmann, P., Westall, F., 2013. Effect of grain size distribution on Raman analyses and the consequences for in situ planetary missions. J. Raman Spectrosc. 44 (6), 916–925.
Foucher, F., Ammar, M.R., Westall, F., 2015. Revealing the biotic origin of silicified Precambrian carbonaceous microstructures using Raman spectroscopic mapping, a potential method for the detection of microfossils on Mars. J. Raman Spectrosc. 46, 873–879.
Grotzinger, J.P., Crisp, J., Vasavada, A.R., Anderson, R.C., Baker, C.J., Barry, R., Blake, D.F., Conrad, P., Edgett, K.S., Ferdowski, B., Gellert, R., Gilbert, J.B., Golombek, M., Gomez-Elvira, J., Hassler, D.M., Jandura, L., Litvak, M., Mahaffy, P., Maki, J., Meyer, M., Malin, M.C., Mitrofanov, I., Simmonds, J.J., Vaniman, D., Welch, R.V., Wiens, R.C., 2012. Mars science laboratory Mission and science investigation. Space Sci. Rev. 170, 5–56.
Grotzinger, J.P., Sumner, D.Y., Kah, L.C., Stack, K., Gupta, S., Edgar, L., Rubin, D., Lewis, K., Schieber, J., Mangold, N., Milliken, R., Conrad, P.G., Des Marais, D., Farmer, J., Siebach, K., Hurowitz, J., McLennan, S.M., Ming, D., Vaniman, D., Crisp, J., Vasavada, A., Edgett, K.S., Malin, M., Blake, D., Gellert, R., Mahaffy, P., Wiens, R.C., Maurice, S., Grant, J.A., Wilson, S., Anderson, R.C., Beegle, L., Arvidson, R., Hallet, B., Sletten, R.S., Rice, M., Griffes, J., Ehlmann, B., Anderson, R. B., Bristow, T.F., Dietrich, W.E., Dromart, G., Eigenbrode, J., Fraeman, A., Hardgrove, C., Herkenhoff, K., Jandura, L., Kocurek, G., Lee, S., Leshin, L.A., Leveille, R., Limonadi, D., Maki, J., McCloskey, S., Meyer, M., Minitti, M., Newsom, H., Oehler, D., Okon, A., Palucis, M., Parker, T., Rowland, S., Schmidt, M., Squyres, S., Steele, A., Stolper, E., Summons, R., Treiman, A., Williams, R., Yingst, A., Team, M.S., 2014. A habitable fluvio-lacustrine environment at Yellowknife Bay, Gale Crater, Mars. Science 343,, 1242777-1–14.
Hauer, P., Grand, J., Djorovic, A., Willmott, G.R., Le Ru, E.C., 2016. Spot size engineering in microscope-based laser spectroscopy. J. Phys. Chem. C 120, 21104–21113.
Hickman-Lewis, K., Foucher, F., Pelletier, S., Messori, F., Westall, F., 2020. Geological appraisals of core samples using the ExoMars 2020 rover instrumentation. Planet. Space Sci. 180, 15.
Hviid, S.F., Madsen, M.B., Gunnlaugsson, H.P., Goetz, W., Knudsen, J.M., Hargraves, R. B., Smith, P., Britt, D., Dinesen, A.R., Mogensen, C.T., Olsen, M., Pedersen, C.T., Vistisen, L., 1997. Magnetic properties experiments on the Mars pathfinder Lander: preliminary results. Science 278, 1768–1770.
Jehlicka, J., Edwards, H.G.M., Vitek, P., 2009. Assessment of Raman spectroscopy as a tool for the non-destructive identification of organic minerals and biomolecules for Mars studies. Planet. Space Sci. 57, 606–613.
Jiang, M., Ammigan, K., Lolov, G., Pellemoine, F., Liu, D., 2023. A novel method for quantifying irradiation damage in nuclear graphite using Raman spectroscopy. Carbon 213, 118181.
Keating, A., Mohammadzadeh, A., Nieminen, P., Maia, D., Coutinho, S., Evans, H., Pimenta, M., Huot, J.-P., Daly, E., 2005. A model for Mars radiation environment characterization. IEEE Trans. Nucl. Sci. 52, 2287–2293.
Kereszturi, A., Bradak, B., Chatzitheodoridis, E., Ujvari, G., 2016. Indicators and methods to understand past environments from ExoMars rover drills. Origin Life Evol. Biospheres 46, 435–454.
Klein, H., Lederberg, J., Rich, A., Horowitz, N.H., Oyama, V.I., Levin, V., 1976. The Viking Mission search for life on Mars. Nature 262, 24–27.
Kminek, G., Bada, J., 2006. The effect of ionizing radiation on the preservation of amino acids on Mars. Earth Planet. Sci. Lett. 245, 1–5.
Le Deit, L., Flahaut, J., Quantin, C., Hauber, E., Mège, D., Bourgeois, O., Gurgurewicz, J., Massé, M., Jaumann, R., 2012. Extensive surface pedogenic alteration of the Martian Noachian crust suggested by plateau phyllosilicates around Valles Marineris. J. Geophys. Res. 117, 25. E00J05.
Le Postollec, A., Incerti, S., Dobrijevic, M., Desorgher, L., Santin, G., Moretto, P., Vandenabeele-Trambouze, O., Coussot, G., Dartnell, L., Nieminen, P., 2009. Monte Carlo simulation of the radiation environment encountered by a biochip during a space Mission to mars. Astrobiology 9 (3), 311–323.
Lee, J., Song, J., Lee, D., Pang, Y., 2019. Metal-enhanced fluorescence and excited state dynamics of carotenoids in thin polymer films. Sci. Rep. 9, 3551.
Mangold, N., Gupta, S., Gasnault, O., Dromart, G., Tarnas, J.D., Sholes, S.F., Horgan, B., Quantin-Nataf, C., Brown, A.J., Le Mouélic, S., Yingst, R.A., Bell, J.F., Beyssac, O., Bosak, T., Calef, F., Ehlmann, B.L., Farley, K.A., Grotzinger, J.P., Hickman-Lewis, K., Holm-Alwmark, S., Kah, L.C., Martinez-Frias, J., McLennan, S.M., Maurice, S., Nuñez, J.I., Ollila, A.M., Pilleri, P., Rice, J.W., Rice, M., Simon, J.I., Shuster, D.L., Stack, K.M., Sun, V.Z., Treiman, A.H., Weiss, B.P., Wiens, R.C., Williams, A.J., Williams, N.R., Williford, K.H., 2021. Perseverance rover reveals an ancient delta-lake system and flood deposits at Jezero crater, Mars. Science 374, 711–717.
Mao, W., Fu, X., Wu, Z., Zhang, J., Ling, Z., Li, B., 2022. The color centers in halite induced by Martian dust activities. Earth Planet. Sci. Lett. 578, 117302.
des Marais, D.J., 2010. Exploring Mars for Evidence of Habitable Environments and Life. Proc. Am. Philos. Soc., 154, pp. 402–421.
Marshall, C.P., Edwards, H.G.M., Jehlicka, J., 2010. Understanding the application of Raman spectroscopy to the detection of traces of life. Astrobiology 10 (2), 229–243.
McKay, C.P., 1997. The search for life on Mars. In: Origin Life Evol. Biosphere, 27, pp. 263–289.
McKenna-Lawlor, S., Gonçalves, P., Keating, A., Morgado, B., Heynderickx, D., Nieminen, P., Santin, G., Truscott, P., Lei, F., Foing, B., Balaz, J., 2012a. Characterization of the particle radiation environment at three potential landing sites on Mars using ESA'S MEREM models. Icarus 218, 723–734.
McKenna-Lawlor, S., Goncalves, P., Keating, A., Reitz, G., Matthiä, D., 2012b. Overview of energetic particle hazards during prospective manned missions to Mars. Planet. Space Sci. 63–64, 123–132.
Patel, M.R., Bérces, A., Kerékgyarto, T., Ronto, G., Lammer, H., Zarnecki, J.C., 2004. Annual solar UV exposure and biological effective dose rates on the Martian surface. Adv. Space Res. 33, 1247–1252.
Pavlov, A.A., Vasilyev, G., Ostryakov, V.M., Pavlov, A.K., Mahaffy, P., 2012. Degradation of the organic molecules in the shallow subsurface of Mars due to irradiation by cosmic rays. Geophys. Res. Lett. 39, 2012GL052166.
Poch, O., Kaci, S., Stalport, F., Szopa, C., Coll, P., 2014. Laboratory insights into the chemical and kinetic evolution of several organic molecules under simulated Mars surface UV radiation conditions. Icarus 242, 50–63.
Poulet, F., Bibring, J.-P., Mustard, J.F., Gendrin, A., Mangold, N., Langevin, Y., Arvidson, R.E., Gondet, B., Gomez, C., Team, T.O, 2005. Phyllosilicates on Mars and implications for early martian climate. Nature 438, 623–627.
Quantin-Nataf, C., Carter, J., Mandon, L., Thollot, P., Balme, M., Volat, M., Pan, L., Loizeau, D., Millot, C., Breton, S., Dehouck, E., Fawdon, P., Gupta, S., Davis, J., Grindrod, P.M., Pacifici, A., Bultel, B., Allemand, P., Ody, A., Lozach, L., Broyer, J., 2021. Oxia Planum: the landing site for the ExoMars "Rosalind Franklin" rover Mission: geological context and Prelanding interpretation. Astrobiology 21 (3), 345–366.
Ranjan, S., Wordsworth, R., Sasselov, D.D., 2017. Atmospheric constraints on the surface UV environment of Mars at 3.9 Ga relevant to prebiotic chemistry. Astrobiology 17 (8), 687–708.
Rull Pérez, F., Martinez-Frias, J., 2006. Raman spectroscopy goes to Mars. Spectrosc. Eur. 18, 18–21.
Rull, F., Maurice, S., Hutchinson, I., Moral, A., Perez, C., Diaz, C., Colombo, M., Belenguer, T., Lopez-Reyes, G., Sansano, A., Forni, O., Parot, Y., Striebig, N., Woodward, S., Howe, C., Tarcea, N., Rodriguez, P., Seoane, L., Santiago, A., Rodriguez-Prieto, J.A., Medina, J., Gallego, P., Canchal, R., Santamaria, P., Ramos, G., Vago, J.L., on behalf of the R.T, 2017. The Raman Laser Spectrometer for the ExoMars rover Mission to Mars. Astrobiology 17 (6-7), 627–654.
Saubenova, M., Rapoport, A., Venkatachalam, M., Dufossé, L., Yermekbay, Z., Oleinikova, Y., 2024. Production of carotenoids by microorganisms. Fermentation 10, 502.
Schulze-Makuch, D., Fairén, A.G., Davila, A.F., 2008. The case for life on Mars. Int. J. Astrobiol. 7, 117–141.
Sonnenfeld, P., 1995. The color of rock salt - a review. Sediment. Geol. 94, 267–276.
Steele, S.C., Fu, R.R., Volk, M.W.R., North, T.L., Brenner, A.R., Muxworthy, A.R., Collins, G.S., Davison, T.M., 2023. Paleomagnetic evidence for a long-lived, potentially reversing martian dynamo at ~3.9 Ga. Sci. Adv. 9, eade9071.
Synytsya, A., Alexa, P., De Boer, J., Loewe, M., Moosburger, M., Würkner, M., Volka, K., 2007. Raman spectroscopic study of calf thymus DNA: an effect of proton- and γ-irradiation. J Raman Spectrosc. 38, 1406–1415.
Takigawa, A., Asada, Y., Nakauchi, Y., Matsumoto, T., Tsuchiyama, A., Abe, M., Watana, N., 2019. H+ ion irradiation experiments of enstatite: space weathering by solar wind. Presented at the 82nd Annual Meeting of The Meteoritical Society 2019, p. 6331.
Vago, J.L., Westall, F., Teams, Pasteur Instrument, Landing, S., Coates, A.J., Jaumann, R., Korablev, O., Ciarletti, V., Mitrofanov, I., Josset, J.-L., De Sanctis, M.C., Bibring, J.-P., Rull, F., Goesmann, F., Steininger, H., Goetz, W., Brinckerhoff, W., Szopa, C., Raulin, F., Westall, F., Edwards, H.G.M., Whyte, L.G., Fairén, A.G., Bibring, J.-P., Bridges, J., Hauber, E., Ori, G.G., Werner, S., Loizeau, D., Kuzmin, R.O., Williams, R. M.E., Flahaut, J., Forget, F., Vago, J.L., Rodionov, D., Korablev, O., Svedhem, H., Sefton-Nash, E., Kminek, G., Lorenzoni, L., Joudrier, L., Mikhailov, V., Zashchirinskiy, A., Alexashkin, S., Calantropio, F., Merlo, A., Poulakis, P., Witasse, O., Bayle, O., Bayón, S., Meierhenrich, U., Carter, J., García-Ruiz, J.M., Baglioni, P., Haldemann, A., Ball, A.J., Debus, A., Lindner, R., Haessig, F., Monteiro, D., Trautner, R., Voland, C., Rebeyre, P., Goulty, D., Didot, F., Durrant, S., Zekri, E., Koschny, D., Toni, A., Visentin, G., Zwick, M., van Winnendael, M., Azkarate, M., Carreau, C., the ExoMars Project Team, 2017. Habitability on early Mars and the search for biosignatures with the ExoMars rover. Astrobiology 17 (6-7), 471–510.
Vitek, P., Osterrothova, K., Jehlicka, J., 2009. Beta-carotene_A possible biomarker in the Martian evaporitic environment: Raman micro-spectroscopic study. Planet. Space Sci. 57, 454–459.
Westall, F., Foucher, F., Bost, N., Bertrand, M., Loizeau, D., Vago, J.L., Kminek, G., Gaboyer, F., Campbell, K.A., Bréhéret, J.G., Gautret, P., Cockell, C.S., 2015. Biosignatures on Mars: what, where, and how? Implications for the search for Martian life. Astrobiology 15 (11), 998–1029.
Westall, F., Hickman-Lewis, K., Hinman, N., Gautret, P., Campbell, K.A., Bréhéret, J.G., Foucher, F., Hubert, A., Sorieul, S., Dass, A.V., Kee, T.P., Georgelin, T., Brack, A., 2018. A hydrothermal-sedimentary context for the origin of life. Astrobiology 18 (3), 259–293.
Westall, F., Hickman-Lewis, K., Cavalazzi, B., Foucher, F., Clodoré, L., Vago, J.L., 2021. On biosignatures for Mars. Int. J. Astrobiol. 20 (6), 1–17.
Winters, Y.D., Lowenstein, T.K., Timofeeff, M.N., 2013. Identification of carotenoids in ancient salt from Death Valley, Saline Valley, and Searles Lake, California, using laser Raman spectroscopy. Astrobiology 13 (11), 1065–1080.
Yamauchi, T., Takada, S., Ichijo, H., Oda, K., 2001. Raman and near-IR study on proton irradiated CR-39 detector and the effect of air-leak on damage formation. Radiat. Meas. 34, 69–73.
Zent, A.P., McKay, C.P., 1994. The chemical reactivity of the Martian soil and implications for future missions. Icarus 108, 146–157.
Ziegler, J.F., Ziegler, M.D., Biersack, J.P., 2010. SRIM – the stopping and range of ions in matter (2010). Nucl. Instrum. Methods Phys. Res., Sect. B 268, 1818–1823.